Journal of Cerebral Blood Flow & Metabolism (2008) 28, 640–652

www.jcbfm.com

The effect of labeling parameters on perfusion-based fMRI in nonhuman primates

Anne C Zappe[1], Josef Pfeuffer[1,2], Hellmut Merkle[3], Nikos K Logothetis[1,4] and Jozien BM Goense[1]

[1]*Department Physiology of Cognitive Processes, Max-Planck Institute for Biological Cybernetics, Tübingen, Germany;* [2]*Siemens Medical Solutions, MR Applications Development, Erlangen, Germany;* [3]*Laboratory of Functional and Molecular Imaging, NIH/NINDS, Bethesda, MD, USA;* [4]*Imaging Science and Biomedical Engineering, University of Manchester, Manchester, UK*

The blood oxygenation level-dependent (BOLD) signal is the most commonly used modality of functional magnetic resonance imaging (fMRI) today. Although easy to implement, it is an ambiguous signal since it results from a combination of several hemodynamic factors. Functional cerebral blood flow changes, as measured by using arterial spin labeling (ASL), typically occur in the parenchyma and have been demonstrated to be more closely coupled to neural activation compared with BOLD. However, the intrinsically low signals from ASL techniques have hindered its widespread application to fMRI for basic research and even more so for clinical applications. Here, we report the first implementation of continuous ASL in the anaesthetized macaque at high magnetic field of 7 T. The technique was optimized to permit maximum signal-to-noise ratio of functional perfusion-based images at high spatial resolution. The effect of labeling parameters, such as label time and post-label delay (*PLD*), on functional cerebral blood flow (fCBF) in the visual cortex was evaluated. Functional cerebral blood flow maps did not change with increasing label time after 2,000 ms, indicating that a label time of 2,000 ms is sufficient for reliable mapping of fCBF. The percent changes obtained using fCBF were better localized to gray matter, than those obtained with BOLD. A short *PLD* of 200 ms revealed significantly higher fCBF changes at the cortical surface, indicating large-vessel contamination, than a long *PLD* of 800 ms. However, the effect of the *PLD* on fCBF was smaller than on baseline CBF. These results are of importance for high-resolution applications, and when accurate quantification is required for studies in monkeys as well as in humans.
Journal of Cerebral Blood Flow & Metabolism (2008) **28,** 640–652; doi:10.1038/sj.jcbfm.9600564; published online 24 October 2007

Keywords: arterial transit time; cerebral blood flow (CBF); monkey brain; specificity; spin tagging (ASL)

Introduction

Because arterial spin labeling (ASL) is capable of non-invasively quantifying regional tissue perfusion, perfusion magnetic resonance imaging with ASL has the potential to become a very important tool with wide applicability in both basic and clinical research. Perfusion-sensitive images are generated by inverting or saturating water protons in the blood vessels supplying the region of interest (ROI), typically in the neck, and measuring the resulting intensity changes in the brain (Detre *et al*, 1992; Dixon *et al*, 1986; Williams *et al*, 1992). After each labeled image, a control image is acquired without labeling. The difference between label and control images yields a signal proportional to the local cerebral blood flow (CBF).

The saturation or inversion procedure is commonly designated as labeling or tagging. Spin tagging can be performed with a broadband radiofrequency (RF) pulse over a thick slab (pulsed ASL—PASL) or with a long RF pulse during the application of a slice-selection gradient (continuous ASL—CASL). The advantage of CASL over PASL is that it has a higher signal-to-noise ratio (SNR) and facilitates quantification as well as multislice imaging (Wang *et al*, 2002; Wong *et al*, 1998). After the tagging of spins, typically a post-label delay (*PLD*) is introduced (Alsop and Detre, 1996) to allow the labeled protons to reach the slice of interest, leave the arteries, and perfuse the tissue. Depending on

Correspondence: Dr AC Zappe, Department of Physiology of Cognitive Processes, Max-Planck Institute for Biological Cybernetics, Spemannstrasse 38, Tübingen 72076, Germany.
E-mail: aczappe@tuebingen.mpg.de
Received 20 March 2007; revised 3 August 2007; accepted 6 September 2007; published online 24 October 2007

the parameter selection, the tissue or arterial fraction of CBF will be emphasized (Detre *et al*, 1994).

Perfusion-based fMRI using ASL (i.e., functional CBF (fCBF)) has certain advantages over the blood oxygenation level-dependent (BOLD) contrast mechanism. The BOLD response reflects a combination of increased CBF and CBV, and decreased oxygen extraction fraction, and its tissue specificity is often reduced by large draining veins that are not spatially confined to the area of neuronal activation (Haacke *et al*, 1994). Experiments in humans (Luh *et al*, 2000) and rats (Duong *et al*, 2000) showed that fCBF is more specific to tissue activation than gradient-echo BOLD. For instance, using fCBF, orientation columns with a spacing of $\sim$1.1 mm could be reliably detected in the visual cortex of cats (Duong *et al*, 2001). Visualization of such structures requires spatial specificity of the functional signal in the submillimeter range. In addition, the quantitative measurements of CBF afforded by ASL facilitate intersubject comparisons, and monitoring of long-term changes within subjects. Last but not least, fCBF can be used to disambiguate the BOLD signal. Davis *et al* (1998), for example, derived a formalism to calculate the cerebral oxygen rate of metabolism ($CMRO_2$) by combining BOLD and CBF measurements. Experiments assessing the individual contributions of CBF, CBV, and $CMRO_2$ to the BOLD signal have therefore been of particular interest for the study of the physiologic basis of BOLD. This kind of BOLD calibration procedure offers yet another very attractive application of perfusion-based fMRI.

Perfusion-based fMRI is not straightforward in its implementation and application. To obtain high-image quality and spatial specificity, the labeling parameters have to be adapted precisely to the specific purpose. For example, *PLD* has to be adapted to the arterial transit time (t_A—the time it takes for the tag to travel from labeling to imaging plane) for the specific subject and ROI. Arterial transit time is different for each species and its physiologic state, and is altered by changes in blood flow such as those caused by anesthetics or hypercapnia. In the absence of a stimulus, for increasing *PLD*, the CBF signal changes from being predominantly located in the arterial compartment (at short *PLD*) to being mostly of capillary origin (for $PLD \approx t_A$). With increasing *PLD*, the signal from the extravascular compartment starts to dominate ($PLD > t_A$). Quantification of CBF typically requires a *PLD* longer than the maximal t_A in the ROI (Alsop and Detre, 1996; Wong *et al*, 1998). However, it is not clear whether the different vascular compartments make the same relative contributions to the fCBF map as to the baseline CBF map. The influence of *PLD* on functional activation was investigated by Gonzalez-At *et al* (2000), who reported a decrease in the t_A by visual and motor activation in humans at 1.5 T. Such a decrease in t_A as a consequence of locally increased CBF does not have to be confined to the area of neural activity. At a resolution of $3.75 \times 3.75 \times 8\,mm^3$ they did not observe differences between the activation maps acquired at different *PLD*. To determine more directly the contribution of intravascular signals to the functional activation maps obtained with CASL, its dependence on labeling parameters has to be determined at higher spatial resolution. We hypothesize that fCBF at short *PLD* will also to some extent be confounded by intravascular signal.

Finally, it is important to optimize ASL given that the inherent low SNR and long measurement duration of ASL have been the main reasons for its limited application in research and medicine. The duration of each scan can be minimized with optimization of the label pulse duration, the so-called label time (*LT*), and *PLD*. An effective remedy to increase SNR is the use of high magnetic field scanners, where the longer T_1 and higher SNR significantly enhance image quality (Duyn *et al*, 2005; Golay and Petersen, 2006). In recent years, the number of high-field magnets has increased dramatically, and attempts to optimally apply ASL in humans have increased at an analogous pace. The implementation of this technique in animals is of equal importance and much development and research has been done in rodents. Here, we report the first successful implementation of CASL in monkeys at 4.7 and 7 T. The monkey model is of undeniable importance in systems neuroscience, as most sensory systems in monkeys and humans are essentially identical, at least with respect to their anatomic and functional organization (Van Essen, 2004). Combined physiology and fMRI experiments promise to bridge the gap between traditional animal electrophysiology and human neuroimaging, as well as to provide insights into the neurovascular coupling (Logothetis *et al*, 2001).

The specific aim of the project was to determine the optimal ASL parameters for the macaque, and to investigate the effect of the labeling parameters on the specificity of fCBF. Continuous ASL was performed with three separate coils to avoid magnetization transfer effects and to enable acquisition of multiple slices (Silva *et al*, 1995; Talagala *et al*, 2004; Zaharchuk *et al*, 1999). The coil setup was optimized for measuring fCBF in the visual cortex of the anesthetized monkey. Parts of this work have been reported in conference proceedings (Zappe *et al*, 2004, 2006).

Materials and methods

Experiments were performed on a vertical 7-T scanner with a 60-cm-diameter bore and a 4.7-T/40-cm-diameter bore scanner (Bruker Medical, Ettlingen, Germany). The 7-T system has a 40 mT/m actively shielded gradient coil with an inner diameter of 33 cm, and rise times $< 200\,\mu s$ (AC44, Siemens Medical Solutions, Erlangen, Germany). The 4.7-T system is equipped with an actively shielded

gradient coil of 26 cm inner diameter that can attain gradients up to 48 mT/m and rise times $<180\,\mu$s. Dedicated primate chairs were used to position the monkeys in the magnets (Logothetis *et al*, 1999; Pfeuffer *et al*, 2004). Five healthy adult monkeys (*Macaca mulatta*, 5 to 8 kg) were used. Altogether 15 experiments (sessions) were acquired on 7 T and 5 on 4.7 T. All experiments were approved by the local authorities (Regierungspräsidium) and were in full compliance with the guidelines of the European Community for the care and use of laboratory animals (EUVD 86/609/EEC). The experiments were performed under general anesthesia according to previously published protocols (Logothetis *et al*, 1999). The animal was sedated with ketamine (15 mg/kg) and intubated after induction with fentanyl (31 mg/kg), thiopental (5 mg/kg), and succinylcholine chloride (3 mg/kg). Anesthesia was maintained with remifentanil (0.5 to 2 μg/kg per min) and mivacurium chloride (3 to 6 mg/kg per h) was used to ensure complete paralysis of the eye muscles. At the beginning of the experiment, each eye was treated with two drops of 1% cyclopentolate hydrochloride to achieve mydriasis and then fitted with hard contact lenses (PMMA-Linsen; Wöhlk, Kiel, Germany) to bring it to focus on the stimulus plane. Lactated Ringer's solution containing 2.5% glucose was infused at 10 mL/kg per h throughout the experiment. Body temperature was maintained at 38 to 39°C.

A three-coil setup for CASL provides improved SNR and reduces magnetization transfer substantially (Silva *et al*, 1995). A saddle coil was used for RF transmission (Pfeuffer *et al*, 2004) in combination with a surface receive coil (40-mm diameter, Bruker BioSpin, Ettlingen, Germany). The surface coil was positioned over one hemisphere of the occipital lobe. For arterial spin labeling, a second ^{1}H-transmit channel was used. A cravat-shaped neck coil (30 mm at smallest loop diameter) was designed to fit the neck of the macaque monkeys (see Figure 1). The adiabatic condition for spin tagging was verified by measuring the B_1-map of the label coil after identifying the location of the left and right carotid and vertebral arteries on an angiography. Decoupling of all three RF coils was actively controlled using PIN diodes built into a self-built logic unit with DC current drivers. Timing was controlled using logic gating signals from the pulse sequence.

The preparation module for ASL consisted of a continuous off-resonance labeling pulse that was applied for a label time (*LT*), in combination with a 2.5 mT/m gradient in the *z* direction, followed by a *PLD*. The power of the labeling pulse was 2.7 W, which was sufficient to achieve a labeling efficiency of 0.85 to 0.9. Label efficiency was determined as described by Talagala *et al* (2004) and Williams *et al* (1992) and has been corrected for T_1 relaxation. To assess magnetization transfer effects, we compared signal intensities in the imaging plane during labeling with off-resonance frequencies of −30,000, −3,000, 0, 3,000, and 30,000 with 3,000 Hz being the proper labeling frequency. To control for superficial heating, we measured the skin temperature in the center of one loop of the labeling coil with a fiberoptic temperature probe (OpSens, Quebec, Canada). Heating effects at the labeling power were within safe limits. In 25 mins of continuous labeling, the skin temperature increased by less than 0.5°C.

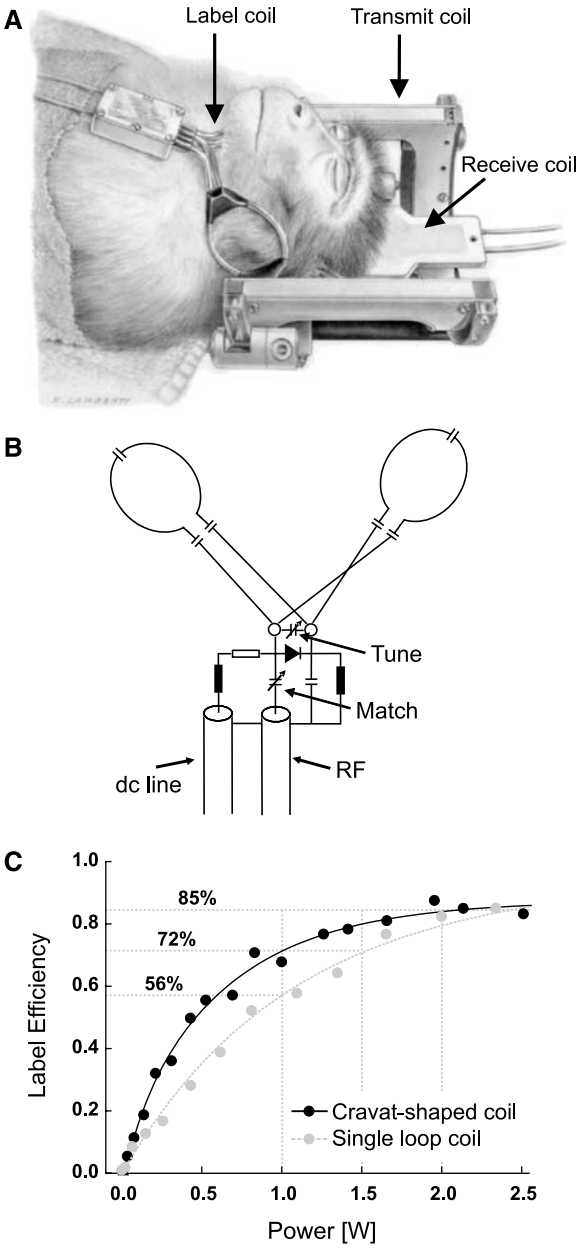

Figure 1 (**A**) Setup of the RF coils in the anaesthetized monkey. All three coils were actively decoupled and powered by a dedicated decoupling unit; (**B**) circuit of the labeling coil and its tune-and-match components. The label coil is cravat shaped to cover both the left- and right-carotid and vertebral arteries; (**C**) label efficiency of a cravat-shaped compared with a single loop coil. The cravat-shaped label coil reaches the maximum label efficiency (0.85) earlier than the single-loop coil.

At 7 T, single-shot, multislice GE-EPI images were acquired with an in-plane resolution of $0.75 \times 0.9\,\text{mm}^2$ and slice thickness of 2 mm. The imaging parameters were TR = 5,300 ms and TE = 14 ms (echo position

25%), matrix = 64 × 64 × 7, flip angle = 90°, and number of repetitions (*NR*) = 64. The EPI readout duration of 42 ms ($< 1.25 \cdot T_2^*$) did not lead to significant T_2^* blurring (Haacke *et al*, 1999). To compare the functional map to the anatomic reference scans, a fully equilibrated reference image (M_0 scan), an inversion recovery series (24 inversion times logarithmically spaced from 50 to 5,000 ms, TR = 8,000 ms) and a high-resolution SE-EPI (TR/TE = 5,000/63 ms) image were acquired. For visual stimulation, two flickering light-emitting diode arrays (red, 8 Hz) placed in front of each eye were used. The stimulus paradigm consisted of four trials (42 s ON/42 s OFF) in total lasting 5.6 mins.

The following sets of functional data were acquired.

(i) *PLD series: PLD* was varied at constant *LT* (*PLD* = 200, 500, 800, and 1,200, *LT* = 3.7 s) (10 sessions, 4 animals);
(ii) *LT-filling series: PLD* and *LT* were varied simultaneously while the sum of *PLD* + *LT* was kept constant (*PLD* = 200, 500, 800 and 1,200 ms, with *LT* 4.7, 4.4, 4.1, and 3.7 s, respectively) (five sessions, two animals);
(iii) *LT series I*: *LT* was varied while *PLD* was kept constant and short (*PLD* = 200 ms, *LT* = 1, 1.5, 2, 2.5, 3, 3.5, and 4s) (five sessions, two animals);
(iv) *LT series II*: *LT* was varied while *PLD* was kept constant and long (*PLD* = 1,000 ms, *LT* = 1, 1.5, 2, 2.5, 3, and 4s) (three sessions, three animals).

Each condition was repeated at least twice during a session, but usually three times. However, due to time constraints not all series could be acquired in a single experiment.

On the 4.7-T scanner we acquired high-resolution CASL data at short and long *PLD* (200 and 800 ms) and constant *LT* of 2 s (five sessions, two animals). Each condition was repeated twice during a session. Eight-segment, multislice GE-EPI images at $0.375 \times 0.333\,mm^2$ in-plane resolution and 2 mm slice thickness were acquired with following parameters: TR/TE = 3,000/11 ms (echo position 30%), EPI readout duration = 15 ms, matrix = 128 × 96 × 5, flip angle = 90°, and *NR* = 64. The stimulus paradigm consisted of eight trials (96 s ON/96 s OFF) in total lasting 25.6 mins. A high-resolution SE-EPI (TR/TE = 3,000/70 ms) was acquired for anatomic reference.

Data Analysis

All data analysis was performed using custom-written Matlab (The MathWorks, Natick, MA, USA) routines. The *k*-space data were corrected for global off-resonance effects to reduce respiration-induced noise (Pfeuffer *et al*, 2002). Thereafter, the data were reconstructed and corrected for Nyquist ghosting when necessary. Cerebral blood flow was calculated by linear surround subtraction, and BOLD was derived by linear surround average as described in Aguirre *et al* (2002). Thus, the temporal resolution of each volume (TR) could be recovered. T_1-maps for CBF quantification were derived by fitting the exponential T_1 decay to the inversion recovery scan using least-square minimization. Quantification of CBF was calculated according to Equation (1) (Wang *et al*, 2002).

$$S = 2\frac{\alpha}{\lambda} f \left\{ \begin{array}{l} T_{1ex} \exp^{-\frac{\delta}{T_{1a}}} \left[\exp^{\frac{\min((\delta - \mathrm{PLD}),0)}{T_{1ex}}} - \exp^{\frac{\delta - \mathrm{LT} - \mathrm{PLD}}{T_{1ex}}} \right] + \\ T_{1a} \left[\exp^{\frac{\min((t_A - PLD),0) - t_A}{T_{1a}}} \right] - \left[\exp^{\frac{\min((\delta - \mathrm{PLD}),0) - \delta}{T_{1a}}} \right] \end{array} \right\} \quad (1)$$

where f = CBF, t_A = arterial transit time, $\alpha = 0.9$ (labeling efficiency), $\lambda = 0.9$ mL blood/g of tissue (brain–blood partition coefficient (Parkes and Tofts, 2002)), $\delta = 1.5$ secs (estimate of transit time from labeling plane to tissue (Parkes and Tofts, 2002)), $T_{1a} = 2.2$ secs (T_1 of arterial blood, (Ewing *et al*, 2001)), $T_{1ex} = 1.85$ secs (T_1 of extravascular tissue (Pfeuffer *et al*, 2004)), S = ASL signal normalized to M_0 (equilibrium tissue magnetization). The normalization to M_0 was done on a voxel-by-voxel basis, to account for the inhomogeneous sensitivity profile of the surface coil.

For the analysis of the functional data ROI were selected. First, the visual cortex was selected manually based on the anatomic scan (because of the sensitivity profile of the surface coil). To include the same voxels in the comparison between conditions, the *t*-maps of each condition were thresholded at $t = 2$ and the least common multiple was used as a mask for all conditions. The number of voxels was derived from the *t*-map of each condition. For fitting of the t_A the average of *t*-maps from all conditions was thresholded at $t = 0.3$. This resulted in a more restrictive mask (fewer non-activated voxels), which was necessary for the fitting procedure. To determine t_A values, ROIs for single sessions and the session-average of the *PLD series* were fitted to Equation (1) while neglecting the *LT* term ($\exp^{\frac{\delta - LT - PLD}{T_{1ex}}}$), because *LT* + *PLD* is sufficiently long. The data set was split into baseline and activated conditions, that is, volumes beginning 5 secs after stimulus onset until the end of stimulus were regarded as activated period (analogously for the baseline period). Then a two-parameter fit (t_A, f) was performed for the activated and baseline period separately, using least-square minimization. Estimate of δ is not critical, because the fit was insensitive to δ within the physiologic range of 1 to 2 secs. The *PLD* was not the same for all slices due to the consecutive acquisition of the slices and a slice timing difference of ~50 ms. The ROI included voxels from all slices to improve SNR and its effective *PLD* was thus an average of the slice-specific *PLD*.

To evaluate the sensitivity of the CBF and BOLD signal to vessels versus gray matter, profiles over the cortical depth were calculated in opercular V1. The profiles were restricted to the operculum of V1 because functional activation was predominantly observed here, and the thickness of cortex and layers is homogeneous over this area.

Profiles of CBF, signal variance in terms of standard deviation (s.d.) and functional activation in the cortex were calculated as described in Goense and Logothetis (2006). During acquisition, slices were oriented perpendicular to the cortical surface, which was confirmed on a sagittal scan. The location of the Gennari line was determined from high-resolution (200 to 250 μm) structural

SE-EPI images (Goense and Logothetis, 2006). The Gennari line serves as an anatomic marker to locate layer IV, and at the same time as a control for partial volume effects, since it is not visible if large partial volume effects are present. Slices with significant partial volume effects (typically the lowest slice) were excluded. For the *PLD series* acquired at 7 T, the in-plane spatial resolution was 0.75 mm A-P and 0.9 mm L-R, which was zero-filled to $0.75 \times 0.75\,mm^2$. The GE-EPI at the 4.7 T were zero-filled to $0.333 \times 0.333\,mm^2$. The lack of gyri in the macaque operculum allows tracing of the cortical surface (using the edge-detection algorithm in Matlab), and fitting a half circle to the boundary (for each slice). Cortical profiles over the activated area were calculated every degree for the 7-T data and every 0.25° for the 4.7-T data. The coordinates specifying the begin- and end-point of each cortical profile were generated from the raw EPI image, and all profiles were calculated between these same points. For the baseline CBF profiles, intensity was normalized to the maximum value within a session to avoid differential weighting of sessions. The fCBF percent change profiles were fitted with a Gauss curve to estimate the full width at half maximum.

Some experiments had to be excluded from the profile analysis because the cortical surface was too uneven to trace because of signal dropout due to susceptibility artifacts from large veins (occurring only at 7 T) or when functional activation in the operculum was too weak. From the 7-T data, profiles were calculated for seven sessions in two animals including five *PLD series* and two *LT-filling* data sets. Because no effect of *LT* on the profiles was observed, all seven sessions were averaged for further analysis. From the 4.7-T data, all sessions were included in the analysis. Error values given are standard error of the mean (s.e.m.) over sessions unless stated otherwise.

Results

For proper labeling of the important arteries on the left and right side a cravat-shaped coil was designed to fit the neck of the monkey (Figure 1). Label efficiencies were calculated at a labeling power of 0 to 2.5 W, and show a superior performance of the cravat shaped over a single-loop label coil. While the maximum label efficiency of 0.85 to 0.9 was similar for both coils, the cravat-shaped coil reached this maximum earlier (Figure 1C). The label coil as well as the transmit and receive coils can be actively detuned to minimize magnetization transfer effects. Changes in signal intensities due to magnetization transfer were below 0.2% of image signal and thus negligible.

Figure 2 shows examples of baseline CBF, fCBF, and BOLD maps acquired with this setup. The CBF maps (Figure 2A) showed clear differences in blood flow in gray and white matter. The short *PLD* of 500 ms resulted in some arterial hotspots. The ASL signal typically constituted 1 to 3% of fully relaxed signal intensity (M_0) in the gray matter of the occipital lobe. The SNR of CBF maps acquired with *LT* of 3.7 secs and *PLD* of 1,200 ms was 28 ± 3 ($n = 11$). Typical CBF values in gray matter were 98 ± 38 mL/100 g per min (mean ± s.d.) and 43 ± 20 mL/100 g per min in white matter (Zappe *et al*, 2007).

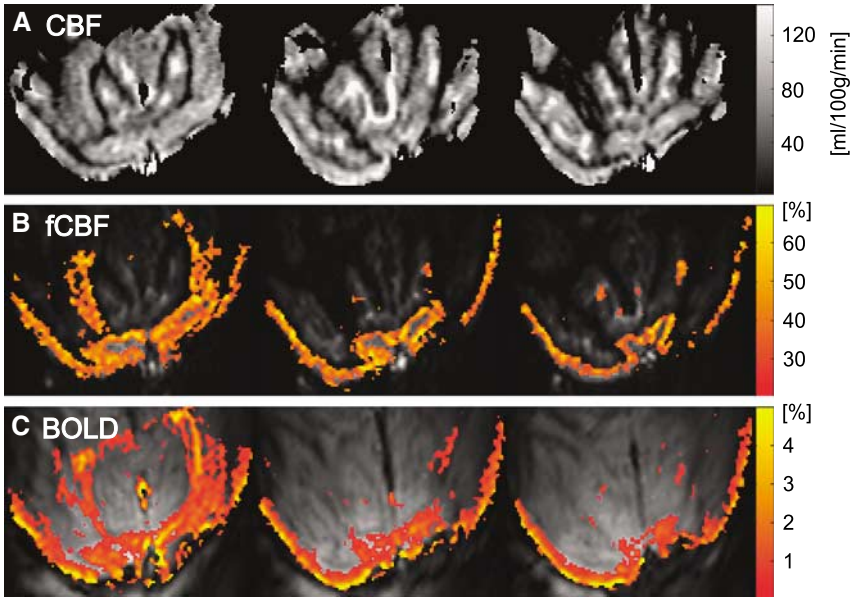

Figure 2 (**A**) Baseline CBF map with *PLD* = 500, *LT* = 2000 ms. Foci of arterial signal can be observed because the *PLD* is shorter than the t_A; (**B**) fCBF map calculated with surround subtraction; (**C**) BOLD map from surround average. The maps (**A**–**C**) are derived from the same scan and have a resolution of $0.9 \times 0.75 \times 2\,mm^3$. Functional activity was mostly localized to gray matter in the primary visual area ($P < 0.05$). Strongest signal and functional activation is observed in the operculum, the stretch of striate cortex at the surface of the brain, where the central 0 to 8° of the visual field are represented.

Functional CBF maps were calculated with surround subtraction and typically showed stimulation-induced changes of 30 to 50% (Figure 2B). Blood oxygenation level-dependent maps (Figure 2C) were calculated from the same images by surround averaging and show robust activation despite the short TE (11 to 14 ms) with typical stimulation-induced changes of 2 to 4%. Comparison of the BOLD and fCBF maps shows that the highest BOLD percent changes occur along the surface of the cortex while highest fCBF changes were located in the center of gray matter.

Effect of Label Time and Post-Label Delay on Functional Cerebral Blood Flow

Theoretically, the ASL signal is expected to increase with increasing *LT* until it saturates after approximately three times T_1 (Detre *et al*, 1992). Figure 3 shows the time course of the ASL signal and its functional modulation on visual stimulation for different *LT*, at a short (Figure 3A, *PLD* = 200 ms) and long *PLD* (Figure 3B, *PLD* = 1,000 ms). The ASL signal increases significantly with *LT* (Table 1), but seems to saturate at 4 s while the stimulus-induced ASL-signal modulation remains constant from *LT* = 2 s to 4 s. Because the baseline ASL signal continues to increase for $LT \geq 2$ s while functional ASL signal modulation remains constant, the percent change shows a tendency to decrease with increasing *LT* for the *LT series I* (*PLD* = 200 ms), whereas there is no such trend for the *LT series II* (*PLD* = 1,000 ms). The number of activated voxels with $t > 2$ also increases for *LT* up to 2 s, and then remains constant for both *PLD*. Mean *t*-values become larger with increasing *LT*. However, except for the change in baseline ASL signal and *t*-values, most changes are not significant, as can be seen in Table 1. In summary, SNR and *t*-values are low up to *LT* = 2 s and show no changes for *LT* > 2 s, suggesting that labeling times need not be longer than *LT* = 2 s.

In a second set of data, the influence of *PLD* on fCBF was investigated. At first, we estimated t_A and CBF during activated and baseline condition by fitting baseline and activated data separately to a two-compartment model (Gonzalez-At *et al*, 2000). Figure 4 shows the fit to the averaged data (10 sessions, 4 animals), which resulted in $t_A = 780 \pm 120$ ms (mean ± confidence interval of 95%) and CBF = 115 ± 56 mL/g per min for the activated condition, and $t_A = 820 \pm 80$ ms with CBF = 91 ± 29 mL/g per min for the baseline condition. Table 2 shows the results of fitting each session separately, which resulted in $t_A = 784 \pm 70$ ms and CBF = 113 ± 6 mL/g per min under activated and $t_A = 855 \pm 80$ ms and CBF = 91 ± 6 mL/g per min under baseline condition. Δt_A differs with 71 ± 40 ms between baseline and activated condition while CBF increases with 25% ± 4% in the activated state. Taking the slice-specific

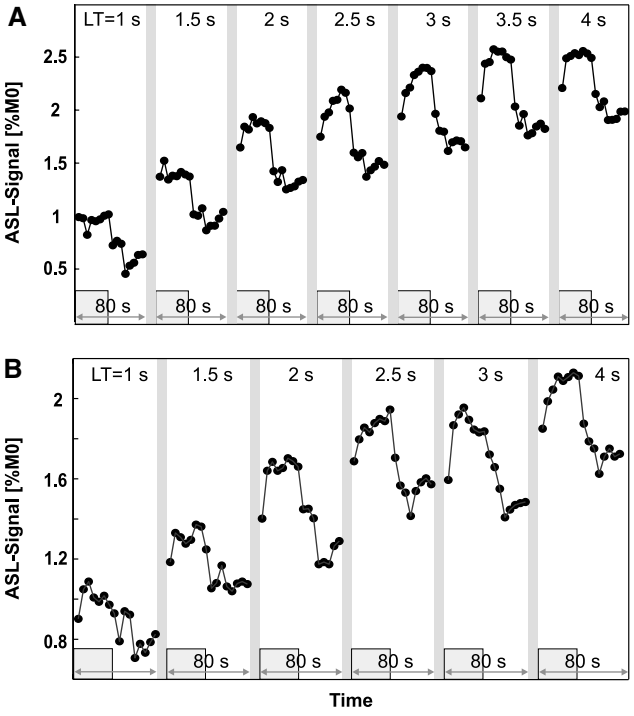

Figure 3 Time course of the average fCBF signal as a function of label time during visual stimulation in V1 for (**A**) *PLD* = 200 ms (five sessions, two animals); (**B**) *PLD* = 1,000 ms (three sessions, three animals). Lower gray boxes indicate the duration of the visual stimulus. Twelve trials per session were averaged for each time course. Although baseline CBF kept increasing, the stimulus-induced CBF modulation remained stable for *LT* > 2,000 ms. See Table 1 for a summary of the data.

PLD into account in the fitting resulted in longer t_A values (within 1 s.d.) and larger confidence intervals while CBF was not affected. Although CBF increases in all 10 sessions (between 8% and 43%), the stimulus-induced difference of t_A and CBF did not reach significance.

The time courses for fCBF at varying *PLD* (200 to 1,200 ms) are shown in Figure 5 (*LT* = 3.7 s). Quantification of the data is shown in Table 3a. Additionally an *LT-filling series* (Table 3b) was acquired, with *LT* and *PLD* covarying while keeping TR constant (*LT* = 3.7 to 4.7 s, *PLD* = 200 to 1,200 ms). We searched for the most efficient ASL protocol, but the results show that the *LT-filling series* closely resembles the *PLD series*, indicating that for an LT of 3.7 s the effect of labeling an additional 1 s is small. For both series, the baseline ASL signal shows a downward trend with increasing *PLD*, which reaches significance between the shortest and longest *PLD*, as is expected based on signal loss due to T_1 at long *PLD* (Gonzalez-At *et al*, 2000). The fCBF percent change were not modulated much by PLD. The *t*-values showed a tendency to decrease, which was significant in the *PLD series* but not in the *LT-filling* series (compare Table 3). The mean

Table 1 Effect of LT on fCBF acquired at two different PLD (200 and 1,000 ms)

(a) LT series I, PLD = 200 ms (five sessions, two animals)

LT (s)	*ASL signal (%M_0)*	*fASL mod. (%M_0)*	*% change*	t-*value*	*Number of voxels*
1	0.6±0.1	0.3±0.1	58±16	1.0±0.3	810±240
1.5	0.9±0.1*	0.4±0.1	48±9	1.3±0.2	890±200
2	1.3±0.1*	0.6±0.1	45±10	1.7±0.3*	990±190
2.5	1.5±0.2*	0.6±0.1	42±8	1.6±0.3*	1040±180
3	1.7±0.2*	0.6±0.1	39±8	1.7±0.4*	1050±260*
3.5	1.8±0.3*	0.7±0.1	37±8	1.9±0.3*	1050±170
4	2.0±0.2*	0.6±0.1	29±9*	1.6±0.5	1010±280

(b) LT series II, PLD = 1,000 ms (three sessions, three animals)

LT (s)	*ASL signal (%M_0)*	*fASL mod (%M_0)*	*% change*	t-*value*	*Number of voxels*
1	0.8±0.4	0.3±0.1	33±15	1.0±0.1	830±120
1.5	1.1±0.5	0.4±0.1	32±12	0.9±0.2	710±210
2	1.3±0.6	0.6±0.1	41±10	1.5±0.1*	1130±170*
2.5	1.5±0.8	0.6±0.1	32±10	1.3±0.1	1070±100*
3	1.5±0.8	0.6±0.1	31±8	1.3±0.1*	1170±160
4	1.8±0.9	0.6±0.1	30±11	1.5±0.1*	1200±150

ASL, arterial spin labeling; fASL, functional ASL; fCBF, functional cerebral blood flow; LT, label time; PLD, post-label delay; ROI, region of interest.
ASL signal, functional ASL-signal modulation (fASL mod.), percent change and *t* values were calculated from the same ROI in V1 for the different conditions. The error is given in s.e.m.
*Depicts significant changes from the value with LT = 1 s at $P < 0.05$ (paired *t*-test).

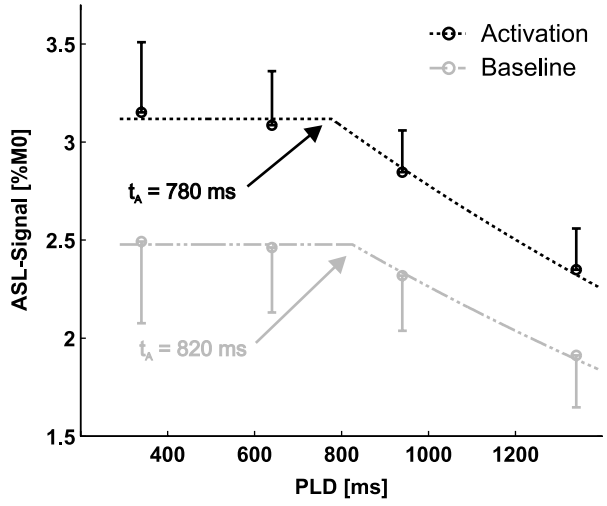

Figure 4 ASL signal as a function of *PLD* fitted with a two-compartment model for activated (black) and baseline condition (gray) ($LT = 3.7$ s). The knee of the curve determines t_A. The results for t_A are in agreement with the average of the single session fits in Table 2 ($t_A = 784 \pm 70$ ms under and 855 ± 80 ms under baseline condition). The error bar shows the s.e.m. (ten sessions, four animals).

t-values for the *LT*-filling series are similar to the *PLD* series, but it is possible that because there are fewer sessions, the difference does not reach significance here. The number of activated voxels did not change significantly between *PLD* conditions. The percent change is constant for most conditions in the *PLD* series and *LT*-filling series, with a significant difference in the *PLD* series between 200 and 500 ms. In summary, this indicates there is no major effect of *PLD* on fCBF in V1 at this resolution when metrics based on a large ROI are used.

Effect of Post-Label Delay on Functional Cerebral Blood Flow Specificity

Because baseline CBF is located primarily in vessels at short *PLD*, it is plausible that fCBF is also located in vessels at short *PLD*. Because ROI analysis is not sensitive to such differences, we determined profiles of the functional activity over the depth of the cortex in V1 operculum. These cortical profiles show that fCBF is more specific than the BOLD signal to gray matter. This is already visible in the functional maps in Figure 2 and becomes evident in Figure 6. The maximum fCBF percent change occurs in the middle of gray matter, with the peak corresponding to roughly layer IV, which is located at 0.8 to 1.4 mm depth. The maximum fCBF percent change $31 \pm 3\%$ occurred at 0.75 mm depth for $PLD = 200$ ms and for $PLD = 1{,}200$ ms a maximum of $24 \pm 5\%$ was located at 1.1 mm depth (Figure 6A). In contrast, the BOLD profiles derived from the same scans peaked at the surface (Figure 6B). The BOLD percent signal change was between $1.9 \pm 0.3\%$ and $2.3 \pm 0.3\%$ at the surface, decreasing to approximately 0.8 ± 0.3 beyond 2.2 mm depth.

The full width at half maximum of the fCBF profiles derived with different *PLD* decreased from

Table 2 Arterial transit times and CBF derived from a separate fit of baseline and activated ASL signal (four different PLD)

Session	*C06.Gw1*	*H02.Gi1*	*O02.uB1*	*I02.uO1*	*I02.vD1*	*I02.vg1*	*I02.v21*	*I02.wh1*	*I02.ut1*	*I02.ww1*
Baseline t_A (ms)	480±280	680±20	1100±550	770±800	730±620	1340±310	1120±70	760±320	760±190	810±70
Activated t_A (ms)	480±200	510±170	1120±700	710±680	640±510	1100±210	860±390	740±130	830±230	850±290
Baseline CBF (ml/g/min)	135±20	98±46	105±54	73±1	70±10	94±50	92±100	93±44	64±57	88±74
Activated CBF (ml/g/min)	151±17	125±34	122±42	94±3	95±13	101±90	112±47	124±61	92±60	118±57

ASL, arterial spin labeling; CBF, cerebral blood flow; PLD, post-label delay.
The error gives the confidence interval (95%) of the fitting procedure. An average $t_A = 855 \pm 80$ ms, and CBF = 91±6 ml/g per min under baseline and $t_A = 784 \pm 70$ ms and CBF = 113±6 ml/g per min under activated condition. The t_A difference between baseline and activated conditions was $\Delta t_A = 71 \pm 40$ ms while ΔCBF = 25±4%.

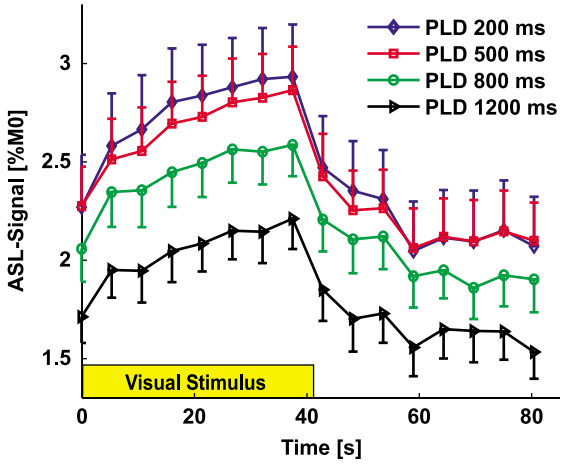

Figure 5 Functional CBF time courses for different *PLD* in primary visual area (*LT* = 3.7 s). Baseline ASL signal decreased with *PLD*, but the stimulus-induced modulation of CBF is similar. No post-stimulus undershoot was observed at this temporal resolution (*TR* = 5,300 ms). See Table 3 for quantification. The error bar shows the s.e.m. (ten sessions, four animals).

1.5 to 1.3 mm with increasing *PLD*, which was observed in all sessions ($P = 0.06$). The peak of the percent change profiles moved slightly inward for increasing *PLD* from 0.7 to 1.1 mm ($P = 0.04$). Although the data suggest that spatial localization of functional activation depends on the *PLD*, these results are only at the border of significance. It appears that the effect of *PLD* is subtle and cannot be easily resolved at the spatial resolution of 0.75×0.9 mm. Therefore, we investigated the effect of *PLD* (for *PLD* = 200 and 800 ms) at a higher resolution ($0.375 \times 0.333 \times 2\,mm^3$) using data acquired at 4.7 T. Figure 7 shows baseline CBF maps (Figures 7A and 7B) and fCBF percent change maps (Figures 7D and 7E) for an example session. In the baseline CBF map at short *PLD* (Figure 7A), foci with high intensity on the edge of cortex are clearly visible, which indicate arterial CBF signal. In the fCBF map at *PLD* = 200 ms, highest percent changes are also localized at the surface (Figure 7D). At a *PLD* of 800 ms both baseline CBF and functional CBF are distributed more homogeneously throughout the cortex (Figure 7E). The higher contribution of the surface vessels at *PLD* = 200 ms, is better visible in the cortical profiles of both baseline (Figure 7C) and fCBF (Figure 7F) (averaged over five sessions from two animals). The ratio of surface fCBF signal to layer IV signal is significantly higher at short *PLD* than at long *PLD* ($P < 0.005$, paired *t*-test). Similarly, in the baseline ASL signal, layer IV signal is significantly higher at short *PLD* than at long *PLD* ($P < 0.02$, paired *t*-test).

The distribution of noise as a function of cortical depth is evaluated in terms of s.d. of the ASL signal and GE-EPI after surround average, and is strongly depth-dependent (Figures 7G and 7H), as has been observed for GE-EPI (Pelled and Goelman, 2004). The highest s.d. was observed at the surface both for ASL signal and GE-EPI, which is likely to be caused by the larger signal variability in the superficial vessels. While the s.d. of the ASL signal remains rather constant in gray matter and only decreases at the white matter border, the s.d. for GE-EPI decreases within gray matter steeply to 20% of the surface level. The s.d. of the GE-EPI does not show a peak around layer IV, as shown by Pelled and Goelman (2004), which could be due to the very short TE of 11 ms. For the ASL signal, the s.d. is significantly higher at the surface for the short *PLD* ($P < 0.05$, paired *t*-test), a result of the larger surface contribution at *PLD* of 200 ms. In summary, ASL maps with a short *PLD* have higher baseline signal, percent change, and noise in the superficial layers than ASL maps with a long *PLD*.

Discussion

The present report, including earlier publication (Zappe *et al*, 2004, 2006), is the first comprehensive implementation of CASL in the nonhuman primate, showing fCBF induced by sensory stimulation. Continuous ASL has been implemented in small animals, humans (Calamante *et al*, 1999), and recently in monkeys at 3 T (Zhang *et al*, 2007), who showed hypercapnia-induced CBF changes. The high SNR of the 7-T and 4.7-T systems and the extensive optimization of the coil setup allowed us

Table 3 Effect of PLD on fCBF acquired with (a) *PLD* between 200 to 1,200 ms and *LT* = 3,700 ms and (b) *PLD* between 200 to 1,200 ms and *LT* between 4,700 to 3,700 ms

(a) PLD series (10 sessions, 4 animals)

LT/PLD (ms)	*ASL signal (%M_o)*	*fASL mod. (%M_o)*	*% change*	t-*value*	*Number of voxels*
3700/200	2.1±0.2	0.7±0.1	34±5	1.8±0.2	1150±200
3700/500	2.1±0.1	0.6±0.1	28±4*	1.6±0.2	1050±170
3700/800	1.9±0.1	0.5±0.1	28±4	1.4±0.2*	980±140
3700/1200	1.6±0.1*	0.45±0.1	29±4	1.3±0.2*	910±120

(b) LT-filling series (five sessions, two animals)

LT/PLD (ms)	*ASL signal (%M_o)*	*fASL mod. (%M_o)*	*% change*	t-*value*	*Number of voxels*
4700/200	2±0.2	0.6±0.1	27±7	1.8±0.4	1780±140
4400/500	1.8±0.3	0.4±0.1	25±6	1.4±0.3	1660±130
4100/800	1.7±0.3	0.5±0.1	30±7	1.5±0.3	1730±110
3700/1200	1.3±0.2*	0.4±0.1	33±6	1.5±0.1	1810±180

ASL, arterial spin labeling; fASL, functional ASL; fCBF, functional cerebral blood flow; LT, label time; PLD, post-label delay; ROI, region of interest.
ASL signal, functional ASL signal modulation (fASL mod.), percent change and *t* values were calculated from the same ROI for the different conditions. The error is given in s.e.m.
*Depicts significant changes from the value with PLD = 200 ms ($P < 0.05$, paired *t*-test).

to obtain functional perfusion maps at submillimeter resolution. To establish perfusion-based functional imaging in the nonhuman primate, the influence of the labeling parameters on fCBF was evaluated. In addition to the labeling parameters, the sequence parameters of the EPI module, such as TE, spatial resolution, and readout duration affect image quality and interpretation of the functional signal, for example by introducing BOLD contamination to the ASL signal. However, because the aim of this study was to determine the effect of labeling parameters on the measured fCBF, we kept the EPI parameters constant. In all analysis we interpolated with surround subtraction as it has been recommended (Aguirre *et al*, 2002) to minimize BOLD contamination, which is an issue at high field where T_2^* of gray matter is as short as 35 ms at 7 T and 42 ms at 4.7 T. Further reduction of BOLD contamination, for example, by using SPIRAL or SE-EPI as readout method is an issue of future studies, since T_2^* can introduce errors in the quantification of CBF (St Lawrence and Wang, 2005) and in functional activation studies (Aguirre *et al*, 2002).

Because a long labeling pulse leads to a long measurement duration and risks tissue heating due to high-power deposition, it is of interest to select the shortest *LT* necessary. Therefore, we investigated the influence of *LT* on fCBF for label pulse durations between 1 and 4 s. For *LT* > 2 s, no significant effect of *LT* on signal modulation, mean *t*-values and number of activated voxels in fCBF maps was found. As the ASL-signal modulation is proportional to stimulus-induced blood flow changes, which should not depend on the ASL parameters, this suggests that an *LT* of 2 s is sufficient for mapping fCBF.

The second important label parameter which affects the duration of CASL scans is the *PLD* after the label pulse. The *PLD* has been introduced in a theoretical framework to account for the effect of arterial transit time on ASL signals (Alsop and Detre, 1996; Zhang *et al*, 1992). When a PLD is shorter than the maximum t_A, the tag has not been delivered homogenously to the parenchyma of all imaged regions. Instead, some labeled signal will still be located in the arteries and the ASL signal from different brain regions will not be proportional to real tissue perfusion. It is not clear how strong the contribution of the PLD is to functional CBF maps despite its apparent effect on baseline CBF. Functional CBF maps are not only affected by heterogeneity in delivery of the tag, as present in the baseline CBF, but also by the heterogeneity in stimulation-induced flow changes in the microcirculation (Villringer *et al*, 1994). The effect of the *PLD* on fCBF has been addressed in humans (Gonzalez-At *et al*, 2000; Mildner *et al*, 2005) to derive arterial transit times, which in fact were shortened by sensory stimuli, however, spatial differences on the fCBF maps were not observed.

In this study, the difference in t_A between the baseline and visually activated conditions was estimated by fitting t_A to four different *PLD* (Figure 3). Compared with the results of Gonzalez-At *et al* (2000), in humans, we found a smaller difference between stimulus and baseline conditions ($\Delta t_A = 70 \pm 40$ ms versus $\Delta t_A = 150 \pm 50$ ms in humans) although our absolute values for t_A were longer than in humans, which aside from having a physiologic origin, could be due to differences in coil design and positioning. The difference in coil positioning between experiments might also

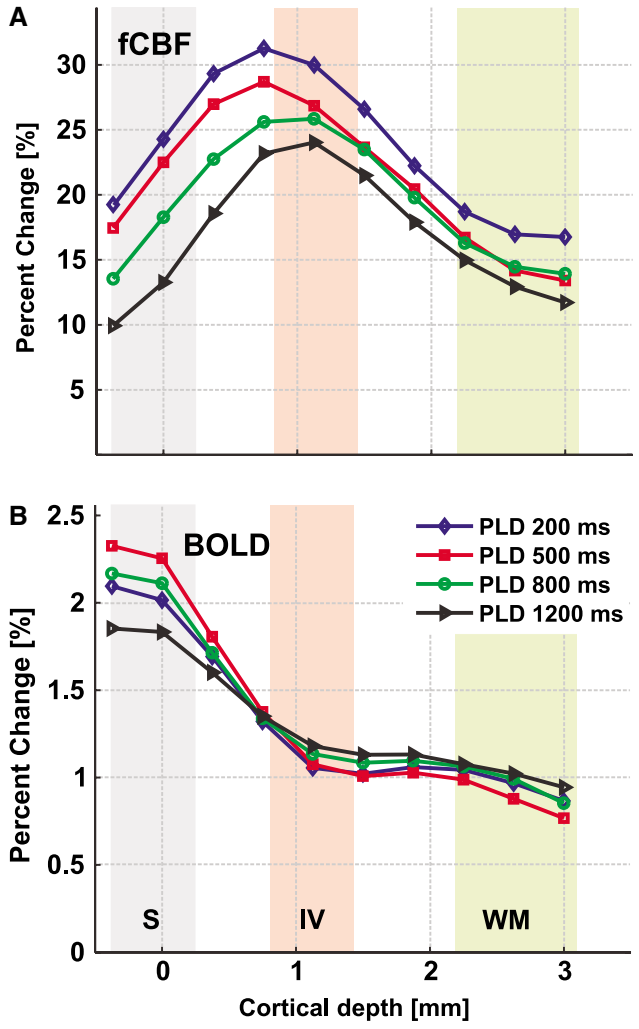

Figure 6 (**A**) Functional CBF profiles and (**B**) BOLD profiles as a function of cortical depth in V1 for different *PLD* with *LT* = 3.7 to 4.7 s (seven sessions, two animals). The percent change of the fCBF signal peaked at a depth of 0.75 to 1.2 mm, while the BOLD percent change was maximal at the surface. Layer IV is located around 0.8 to 1.4 mm depth as determined based on the location of the Gennari line in high-resolution SE-EPI images. S = surface, IV = layer IV, WM = white matter.

account for some of the intersubject and intersession variability in t_A. A more extensive modeling of absolute measures of t_A in the macaque was performed in a different study and determined t_A in gray matter to be 742 ± 184 ms (mean $\pm$ s.d.) at baseline and 682 ± 187 ms during visually activated condition (Zappe *et al*, 2007). Gonzalez-At *et al* (2000) showed that their data were better fitted when assuming a Gaussian distribution of blood velocities instead of plug flow, which resulted in smaller Δt_A. Because in our study only four different *PLD* were acquired, our ability to test different models was limited. Because Δt_A was further decreased with the Gaussian distribution model, these results suggest that the contribution of Δt_A to fCBF signal is smaller in monkeys than in humans.

Table 3 summarizes the effect of the *PLD* on the ASL signal and functional ASL-signal modulation in V1. Both baseline and functional ASL tend to decrease with increasing *PLD*. Although not significant, this indicates a different weighting of the vascular and tissue compartments at different *PLD*. For the baseline CBF, this is well known and has been shown many times (Alsop and Detre, 1996). In addition, this indicates that at short *PLD*, fCBF changes originate in both the arterial and tissue compartment, with higher fCBF changes in the arterial compartment. Percent change, *t*-values, and number of activated voxels are values that are calculated from the ASL signal and ASL-signal modulation, and hence they depend on the baseline ASL signal as well as on the noise in the images. Although a useful measure for image quality and comparison with other studies, these parameters are interdependent, and therefore the interpretation is not straightforward. The monotonic decrease of the mean *t*-values with *PLD* shows that, although better localized in the parenchyma, contrast to noise of fCBF at long *PLD* is lower, with the result that activation is more difficult to detect. Because a short *PLD* would be preferable to use for the above-mentioned reasons of decreasing measurement duration and its higher *t*-values, its impact on fCBF needs to be known.

We assess the sensitivity of fCBF to vessels versus gray matter more directly, by calculating the intensity of activation as a function of cortical depth. This is possible in V1 because of the highly structured anatomy of the vascular bed where large pial vessels feed or drain small intracortical arteries and veins that are oriented perpendicularly to the cortical surface (Duvernoy *et al*, 1981; Weber *et al*, 2006). Capillary density varies with neuronal density and is highest around layer IV (Weber *et al*, 2006). Hence, a large functional signal at the surface signifies a larger contribution from large vessels, while in the case that functional activation is predominantly located in gray matter, the large-vessel contribution is decreased, and functional activation can be assumed to be predominantly derived from capillaries and small vessels. In our study, we found that GE-EPI BOLD and fCBF derived from the same scans resulted in very distinct patterns. The largest BOLD changes occurred at the surface, whereas the highest fCBF changes were localized in gray matter and peaked around layer IV. Although the short TE used in this study increases the contribution from large veins, our finding that the BOLD signal is located mostly at the surface agrees with previous results (Lee *et al*, 1999; Duong *et al*, 2000; Zhao *et al*, 2004; Goense and Logothetis, 2006).

Similar to the difference between BOLD and fCBF, any large-vessel contributions at short *PLD* should be evident in the profiles measured at different *PLD*. At a resolution of $0.75 \times 0.9 \times 2\,\text{mm}^3$ at 7 T we were able to resolve small but consistent changes in the

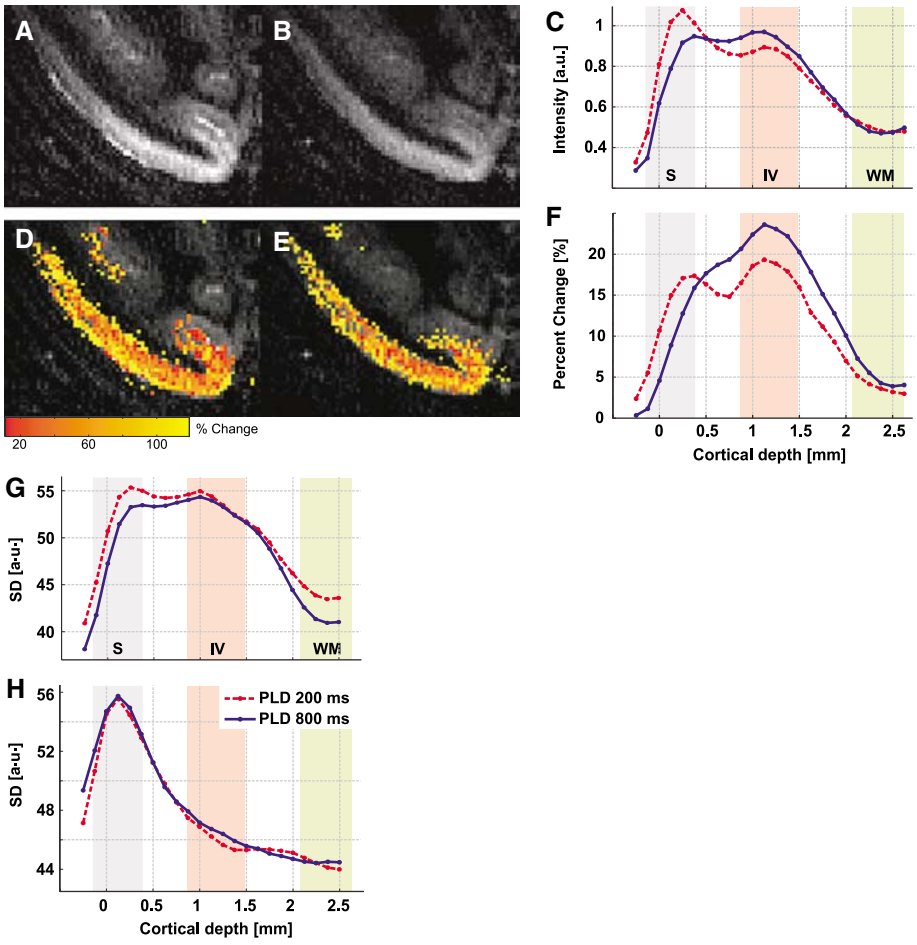

Figure 7 Representative (**A**, **B**) baseline and (**D**, **E**) fCBF maps acquired at two different *PLD*: (**A**, **D**) *PLD* = 200 ms; (**B**, **E**) *PLD* = 800 ms. (**C**) Average cortical depth profile of baseline ASL intensity, and (**F**) percent functional change acquired at *PLD* = 200 (red) and 1,000 ms (blue) (*LT* = 2,000 ms, five sessions, two animals). Large-vessel contribution to both baseline and functional CBF is seen at *PLD* = 200 ms (**A**, **D**, **C**, **F**). At short *PLD*, the ratio of percent functional change at the surface (gray bar) versus in layer IV (pink bar) is higher than at long *PLD* ($P < 0.005$). The same holds for baseline CBF ($P < 0.02$). (**G**) s.d. of baseline CBF and (**H**) s.d. of GE-EPI used for BOLD at *PLD* = 200 ms (red dashed curve) and *PLD* = 800 ms (blue curve). The s.d. at the surface is higher at short *PLD* ($P < 0.05$), indicating larger vessel contribution to the signal. The s.d. for GE-EPI decreases 20% from surface into gray matter with no difference between *PLD*. S = surface, IV = layer IV, WM = white matter.

profiles of fCBF activation for different *PLD*. Because this resolution is somewhat low to clearly visualize differences between vessels and parenchyma, additional data was acquired at a resolution of $0.375 \times 0.333 \times 2\,\text{mm}^3$ at 4.7 T. Although the CASL setup was similar for both data sets, the lower field and shorter TE will lead to a reduced BOLD contamination in the 4.7-T data compared with the 7-T data. T_1 of arterial blood is shorter at lower field (1.7 versus 2.2 secs), which decreases venous signal in the CBF maps. The shorter *LT* (2 versus 3.7 s) reduces the fraction of signal in the gray matter relative to the vessel signal for a short *PLD*. All these effects will lead to an enhancement of the tissue versus vessel difference between *PLD*. In accordance to this, the profiles acquired at 4.7 T clearly show that fCBF at the surface is larger for short *PLD* while at long *PLD*, the fCBF in layer IV is highest. It is not only the case that functional activation is larger at the surface for the short PLD, but also the baseline ASL signal and s.d. of the ASL signal are larger. Depending on the relative contributions of baseline ASL signal and s.d., the large surface signal might be enhanced or not show up in *t*-value maps. The s.d. of the BOLD signal is shown in Figure 7H. Here, the noise profile does not depend on the PLD, instead there is a huge difference of 20% between surface and gray matter which is not present in the ASL signal.

To summarize, in this study we show high-resolution CASL data from the macaque monkey at 4.7 and 7 T, and investigated the effect of the labeling parameters on baseline and functional CBF maps. The results show that fCBF is less sensitive to large-vessel signal than baseline CBF. However, at short *PLD* there is still a significant large-vessel contribution to the fCBF signal. But at spatial resolutions coarser than $1 \times 1 \times 2$ mm, these

differences in specificity are not expected to substantially affect the activation maps. Thus, at lower resolution, and if absolute quantification of fCBF is not required, a shorter *PLD* can be used, leading to substantially decreased acquisition times and increased *t*-values, which facilitates the detection of activation. At high resolution, a long *PLD* is needed to decrease fCBF arising from vessels. In conclusion, whereas *LT* did not have much influence on the strength of the perfusion-based fMRI signal, we showed that the choice of *PLD* does affect the specificity of both baseline- and fCBF signal, particularly at high resolution. This will be of importance in high-resolution applications and when accurate quantification is required for studies in monkeys as well as in humans.

Acknowledgements

We thank our colleagues Kamil Uludag, Bruno Weber, and Alexander Kaiser for many valuable discussions and Mark Augath, Thomas Steudel, and Michael Beyerlein for technical assistance. We are also thankful to Harald Moeller and his colleagues at the MPI of Cognitive Neuroscience in Leipzig, and to Alfonso Silva of NINDS for helpful discussions at the start of this project. This work was supported by the Max-Planck Society and in part (HM) by the Intramural Research Program of the NIH (National Institute Neurological Disorders and Stroke), Bethesda, Maryland.

References

Aguirre GK, Detre JA, Zarahn E, Alsop DC (2002) Experimental design and the relative sensitivity of BOLD and perfusion fMRI. *NeuroImage* 15:488–500

Alsop DC, Detre JA (1996) Reduced transit-time sensitivity in noninvasive magnetic resonance imaging of human cerebral blood flow. *J Cereb Blood Flow Metab* 16:1236–49

Calamante F, Thomas DL, Pell GS, Wiersma J, Turner R (1999) Measuring cerebral blood flow using magnetic resonance imaging techniques. *J Cereb Blood Flow Metab* 19:701–35

Davis TL, Kwong KK, Weisskoff RM, Rosen BR (1998) Calibrated functional MRI: mapping the dynamics of oxidative metabolism. *Proc Natl Acad Sci USA* 95:1834–9

Detre JA, Leigh JS, Williams DS, Koretsky AP (1992) Perfusion imaging. *Magn Reson Med* 23:37–45

Detre JA, Zhang W, Roberts DA, Silva AC, Williams DS, Grandis DJ, Koretsky AP, Leigh JS (1994) Tissue specific perfusion imaging using arterial spin labeling. *NMR Biomed* 7:75–82

Dixon WT, Du LN, Faul DD, Gado M, Rossnick S (1986) Projection angiograms of blood labeled by adiabatic fast passage. *Magn Reson Med* 3:454–62

Duong TQ, Kim D-S, Ugurbil K, Kim S-G (2001) Localized cerebral blood flow response at submillimeter columnar resolution. *Proc Natl Acad Sci USA* 98:10904–9

Duong TQ, Silva AC, Lee SP, Kim SG (2000) Functional MRI of calcium-dependent synaptic activity: cross correlation with CBF and BOLD measurements. *Magn Reson Med* 43:383–92

Duvernoy HM, Delon S, Vannson JL (1981) Cortical blood vessels of the human brain. *Brain Res Bull* 7:519–79

Duyn JH, van Gelderen P, Talagala L, Koretsky A, de Zwart JA (2005) Technological advances in MRI measurement of brain perfusion. *J Magn Reson Imaging* 22:751–3

Ewing JR, Cao Y, Fenstermacher J (2001) Single-coil arterial spin-tagging for estimating cerebral blood flow as viewed from the capillary: relative contributions of intra- and extravascular signal. *Magn Reson Med* 46:465–75

Goense JBM, Logothetis NK (2006) Laminar specificity in monkey V1 using high-resolution SE-fMRI. *Magn Reson Imaging* 24:381

Golay X, Petersen ET (2006) Arterial spin labeling: benefits and pitfalls of high magnetic field. *Neuroimaging Clin N Am* 16:259–68, x

Gonzalez-At JB, Alsop DC, Detre JA (2000) Cerebral perfusion and arterial transit time changes during task activation determined with continuous arterial spin labeling. *Magn Reson Med* 43:739–46

Haacke EM, Brown JW, Thompson L, Venkatesan R (1999) *Magnetic resonance imaging: physical principles and sequence design*. New York: John Wiley & Sons, Inc

Haacke EM, Hopkins A, Lai S, Buckley P, Friedman L, Meltzer H, Hedera P, Friedland R, Klein S, Thompson L, Detterman D, Tkach J, Lewin JS (1994) 2D and 3D high resolution gradient echo functional imaging of the brain: venous contributions to signal in motor cortex studies. *NMR Biomed* 7:54–62

Lee SP, Silva AC, Ugurbil K, Kim SG (1999) Diffusion-weighted spin-echo fMRI at 9.4 T: microvascular/tissue contribution to BOLD signal changes. *Magn Reson Med* 42:919–28

Logothetis NK, Guggenberger H, Peled S, Pauls J (1999) Functional imaging of the monkey brain. *Nat Neurosci* 2:555–62

Logothetis NK, Pauls J, Augath M, Trinath T, Oeltermann A (2001) Neurophysiological investigation of the basis of the fMRI signal. *Nature* 412:150–7

Luh WM, Wong EC, Bandettini PA, Ward BD, Hyde JS (2000) Comparison of simultaneously measured perfusion and BOLD signal increases during brain activation with T(1)-based tissue identification. *Magn Reson Med* 44:137–43

Mildner T, Moller HE, Driesel W, Norris DG, Trampel R (2005) Continuous arterial spin labeling at the human common carotid artery: the influence of transit times. *NMR Biomed* 18:19–23

Parkes LM, Tofts PS (2002) Improved accuracy of human cerebral blood perfusion measurements using arterial spin labeling: accounting for capillary water permeability. *Magn Reson Med* 48:27–41

Pelled G, Goelman G (2004) Different physiological MRI noise between cortical layers. *Magn Reson Med* 52:913–6

Pfeuffer J, Merkle H, Beyerlein M, Logothetis NK, Steudel T (2004) Anatomical and functional MR imaging in the macaque monkey using a vertical large-bore 7 tesla setup. *Magn Reson Imaging* 22:1343–59

Pfeuffer J, Van de Moortele PF, Ugurbil K, Hu X, Glover GH (2002) Correction of physiologically induced global off-resonance effects in dynamic echo-planar and spiral functional imaging. *Magn Reson Med* 47:344–53

Silva AC, Zhang W, Williams DS, Koretsky AP (1995) Multi-slice MRI of rat brain perfusion during amphetamine stimulation using arterial spin labeling. *Magn Reson Med* 33:209–14

St Lawrence KS, Wang J (2005) Effects of the apparent transverse relaxation time on cerebral blood flow measurements obtained by arterial spin labeling. *Magn Reson Med* 53:425–33

Talagala SL, Ye FQ, Ledden PJ, Chesnick S (2004) Whole-brain 3D perfusion MRI at 3.0 T using CASL with a separate labeling coil. *Magn Reson Med* 52:131–40

Van Essen DC (2004) Surface-based approaches to spatial localization and registration in primate cerebral cortex. *NeuroImage* 23(Suppl 1):S97–107

Villringer A, Them A, Lindauer U, Einhaupl K, Dirnagl U (1994) Capillary perfusion of the rat brain cortex. An *in vivo* confocal microscopy study. *Circ Res* 75:55–62

Wang J, Alsop DC, Li L, Listerud J, Gonzalez-At JB, Schnall MD, Detre JA (2002) Comparison of quantitative perfusion imaging using arterial spin labeling at 1.5 and 4.0 Tesla. *Magn Reson Med* 48:242–54

Weber B, Keller AL, Groso A, Stampanoni M, Logothetis NK (2006) Quantitative aspects of the microvascular system in macaque visual cortex. In: *FENS abstracts*, vol 3, A179.27

Williams DS, Detre JA, Leigh JS, Koretsky AP (1992) Magnetic resonance imaging of perfusion using spin inversion of arterial water. *Proc Natl Acad Sci USA* 89:212–6

Wong EC, Buxton RB, Frank LR (1998) A theoretical and experimental comparison of continuous and pulsed arterial spin labeling techniques for quantitative perfusion imaging. *Magn Reson Med* 40:348–55

Zaharchuk G, Ledden PJ, Kwong KK, Reese TG, Rosen BR, Wald LL (1999) Multislice perfusion and perfusion territory imaging in humans with separate label and image coils. *Magn Reson Med* 41:1093–8

Zappe AC, Goense JBM, Merkle H, Pfeuffer J, Logothetis NK (2006) Perfusion-based functional imaging in the monkey brain at 7T—investigations of CASL parameters. In: *Proceedings of the 14th Annual Meeting of ISMRM*. Seattle, USA, 2135

Zappe AC, Pfeuffer J, Logothetis NK (2004) Continuous arterial spin labeling (CASL) setup for the primate brain at 7 T using a three-coil approach. In: *Proceedings of the 21st ESMRMb*. Copenhagen, Denmark, 66–7

Zappe AC, Reichold J, Burger C, Weber B, Buck A, Pfeuffer J, Logothetis NK (2007) Quantification of cerebral blood flow in nonhuman primates using arterial spin labeling and a two-compartment model. *Magn Reson Imaging* 27:775–83

Zhang W, Williams DS, Detre JA, Koretsky AP (1992) Measurement of brain perfusion by volume-localized NMR spectroscopy using inversion of arterial water spins: accounting for transit time and cross-relaxation. *Magn Reson Med* 25:362–71

Zhang X, Nagaoka T, Auerbach E, Champion R, Zhou L, Hu X, Duong T (2007) Quantitative basal CBF and CBF fMRI of rhesus monkeys using three-coil continuous arterial spin labeling. *NeuroImage* 34:1074–83; e-pub 2006 November 1027

Zhao F, Wang P, Kim SG (2004) Cortical depth-dependent gradient-echo and spin-echo BOLD fMRI at 9.4T. *Magn Reson Med* 51:518–24